Tuneable photoconductivity and mobility enhancement in printed MoS$_2$/graphene composites

Adam G. Kelly, Conor Murphy, Andrew Harvey, Amir Sajad Esmaeily, David McCloskey, Jonathan N. Coleman[*]

School of Physics, CRANN and AMBER Research Centers, Trinity College Dublin, Dublin 2, Ireland.

*colemaj@tcd,ie

ABSTRACT: Aiming to increase carrier mobility in nanosheet-network devices, we have investigated MoS$_2$-graphene composites as active regions in printed photodetectors. Combining liquid-exfoliation and inkjet-printing, we fabricated all-printed photodetectors with graphene electrodes and MoS$_2$-graphene composite channels with various graphene mass fractions ($0 \leq M_f \leq 16wt\%$). The increase in channel dark conductivity with M_f was consistent with percolation theory for composites below the percolation threshold. While the photoconductivity increased with graphene content, it did so more slowly than the dark conductivity such that the fractional photoconductivity decayed rapidly with increasing M_f. We propose that both mobility and dark carrier density increase with graphene content according to percolation-like scaling laws while photo-induced carrier density varies only weakly with graphene loading. This leads to percolation-like scaling laws for both photoconductivity and fractional photoconductivity, in excellent agreement with the data. These results suggest that channel mobility and carrier density increase by ~100× on the addition of 16wt% graphene.

Keywords: printed electronics, network devices, transistor

The growing demand for low-cost electronics has sparked a wide investigation into printable, low-performance devices and circuits. The field has developed over the last 25 years from early demonstrations of solution processed devices[1, 2] to today's ability to print integrated circuitry.[3] The most commonly studied materials in this area continue to be organic polymers and molecules which have been used to print in a range of devices, including light-emitting diodes and transistors.[3] However, these materials suffer a number of disadvantages including relatively low mobility and high cost. This has led a number of researchers to investigate the use of printed networks of inorganic nanoparticles and nanotubes in device applications.[4, 5] While good device performance has been demonstrated from these materials (e.g. high mobilities and on:off ratios in printed transistors), it is not clear whether such technologies can be scaled at low cost due to difficulties in materials synthesis and processing.

More recently, it has been shown that 2-dimensional nanosheets are promising candidates for electronic device applications, with single-nanosheet transistors displaying relatively high mobilities and on/off ratios.[6, 7] In the context of printed electronics, fabricating printed nanosheet network-based devices will require access to nanosheet-containing inks. Critically, nanosheets can be produced cheaply in a form amenable to ink formulation by techniques such as liquid-phase exfoliation (LPE).[8, 9] This method uses scalable processes, such as high shear mixing,[9] to exfoliate layered crystals into few-layer nanosheets in appropriate liquids. Using simple, centrifugation-based, post-processing techniques, it is possible to size-select the nanosheets while simultaneously exchanging the solvent and increasing the concentration up to ~10 mg/ml.[10] Crucially, these procedures can be applied to a range of layered materials yielding a host of different nanosheets including graphene, BN, MoS_2, $Ni(OH)_2$, GaS, etc.[8, 11, 12] The combination of exfoliation and post-processing techniques is ideal for producing inks which can be printed into nanosheet network-based devices [13, 14] and a number of network-based printed devices have now been reported. While the emphasis has been on printed photodetectors due to their simplicity,[13, 15-19] memory devices [13] and, more recently, transistors have also been printed.[20]

A key problem with networks composed solely of semiconducting nanosheets is the limited network mobility of ~0.1 cm^2/Vs,[20] relatively low compared to state-of-the-art printed organics which now perform at 10 cm^2/Vs.[3] This limitation is an intrinsic effect of the network itself as the network mobility is restricted by inter-nanosheet junctions.[20] Obvious strategies to address this involve reducing junction resistance, for example by increasing nanosheet overlap at junctions or by chemical modification. Here, we suggest a different approach. Building on

work by Palermo et al,[21] we propose that the mobility of a network of semiconducting nanosheets, such as MoS_2, can be enhanced by adding small quantities of conducting nanosheets such as graphene. The presence of graphene islands in a sea of MoS_2 nanosheets allows carriers to alternate between travelling through MoS_2 and graphene, with the graphene sections acting as high mobility links in the overall conductive path. This would reduce the carrier transit times yielding an increase in effective mobility. This simple procedure to increase mobility may improve the performance of printed nanosheet devices to the point where they are competitive with printed organics.

With this in mind, the aim of this work is three-fold. We aim to demonstrate the feasibility of fabricating all-printed devices with graphene electrodes and MoS_2-graphene channels, focusing on photodetectors for simplicity. We investigate how the addition of graphene affects both the electrical and photoconductive properties of the channel. Finally, we will attempt to use this data to develop an understanding of how the presence of graphene affects generic device properties such as mobility and carrier density.

Graphene and MoS_2 nanosheets were both produced by liquid-phase exfoliation using layered powders as starting materials (Timrex Timcal and Sigma respectively).[19] Briefly, each layered powder was exfoliated in solvent N-methyl-pyrrolidone (NMP) using a horn-tip sonicator (Sonics Vibracell VCX-750) and the resultant dispersion was subjected to liquid cascade centrifugation [10] to define the nanosheet size distributions. The nanosheets were size-selected using a two-step cascade, a procedure often referred to as trapping.[10] We employed a Hettich 220K centrifuge, and for MoS_2, used rotation rates equivalent to 106g and 426g, parameters which should give nanosheets with lateral size of ~200 nm. Such small nanosheets are required to avoid clogging of the nozzle during printing (nozzle size ~20 μm).[14, 19] However, we used slightly different centrifugation conditions for graphene, trapping between 27g and 106g. This should result in larger nanosheets which would be expected to give larger graphene islands in the printed film and so better mobility enhancement. For both MoS_2 and graphene, after the second centrifugation step,[10] the sediments were redispersed in NMP at concentrations of ~1 mg/ml. These procedures resulted in nanosheet/NMP dispersions as shown in Figures 1A and 1B. Representative TEM images of both nanosheet types are shown in Figures 1C and 1D. In all cases, the samples are dominated by few-layer nanosheets with mean lateral sizes of ~650 nm and ~220 nm for graphene and MoS_2 respectively. Although the graphene nanosheets are somewhat larger than the usual limit of one-fiftieth of the nozzle size, we found no problems with printing. The graphene and MoS_2 dispersions were blended to give

a range of composite inks,[22] all with total nanosheet content of ~1 mg/ml, but with the graphene mass fraction ($M_f = M_{graphene} / (M_{graphene} + M_{MoS2})$) varying from 1wt% to 16wt%. Along with the pure graphene and MoS_2 dispersions, these inks were used to print photodetectors in a manner similar to our previous report.[19]

Using the graphene-based ink, pairs of graphene interdigitated electrodes (IDE) (Figure 1E, top) were inkjet printed with a Dimatix DMP 2850. These were designed to have inter-electrode channel dimensions of: length, L=200 μm; width, w=15 mm; depth (i.e. graphene electrode thickness), t=700 nm. Using the same procedure, we then printed an MoS_2 or MoS_2-graphene composite channel on top of each IDE as a 700 nm thick layer (area ~2×5 mm^2) which both filled the inter-electrode trench and covered the surrounding area (Figure 1E, bottom). The channels were printed with a range of graphene mass fractions from 0% (MoS_2-only) to 16wt%. SEM imaging showed the channel/electrode interface to be relatively smooth in all cases with line edge roughness of ~10 μm (Figure 1F). Higher magnification imaging shows the channel region (i.e. the MoS_2 or MoS_2-graphene composite) can be clearly differentiated from the electrode (Figure 1G). Both channel (Figure 1H) and electrodes (Figure 1I) visibly consist of disordered networks of nanosheets with visible porosity.

The electrical resistance (Keithley 2612A) measured (in the dark) for IDE/composite devices is plotted versus the mass fraction of graphene in the composite channel in Figure 2A. While the device with only MoS_2 in the channel (M_f=0) displays a high resistance of ~200 MΩ, the resistance drops significantly as graphene content is increased, reaching ~20 kΩ for the sample with a channel containing M_f=16% graphene. Taking the conductivity of the graphene electrodes as ~10^4 S/m,[23] this implies a series resistance associated with the electrodes of ~ kΩ which is negligible compared to the overall device resistance over most of the compositional range studied here.

Normalising to the channel dimensions, the dark conductivity, σ_D, is plotted versus graphene mass fraction in Figure 2B. The conductivity of the MoS_2-only channel was ~5×10^{-5} S/m, reasonably close to previously measured values.[24] The channel conductivity increased strongly with increasing M_f, reaching ~1 S/m for the 16wt% sample. Previous work [22] on the conductivity of MoS_2/graphene composites has shown a similar increase occurs below the percolation threshold (i.e. the conductive filler loading level where the first continuous conducting path is formed), with a steeper conductivity increase occurring just above the percolation threshold. This will be discussed further below.

We tested the photoresponse of these systems by measuring I-V curves at different incident light intensities for devices with different graphene contents in the channel. The illumination was provided using a λ=511 nm laser and the incident intensity was controlled using neutral density filters. The spot diameter was 3 mm which meant that approximately 55% of the device was illuminated. As a result, the absolute photoconductivity was always slightly lower than would have been the case for complete illumination. Examples of I-V curves for a range of laser intensities are shown in Figures 2E and 2F for two devices, one with an MoS_2-only channel (2E) and one with an MoS_2-graphene (16wt%) channel (2F). While the photoresponse is clearly visible for the MoS_2-only channel, it is much more subtle in the MoS_2/graphene (16wt%) channel (see inset). The channel conductivity, extracted from the slope of the I-V curve around the origin, is shown in Figures 2E and 2F as a function of incident intensity for the two samples described above. In both cases, the conductivity under illumination, σ, increased sublinearly with intensity as observed previously for nanosheet networks.[13, 24] The data is consistent with photoconductivity (i.e. the conductivity increase on illumination) increasing with intensity, I, as: $\sigma - \sigma_D \propto I^{\gamma}$, where γ is a material-dependent constant, as is expected for a trap-limited system.[24] This relationship fitted all the samples well (dashed lines in Figures 2E and 2F) with values of γ ranging between 0.54 and 0.61 (with the exception of one outlier). This is consistent with the previously reported value of 0.54 for in-plane MoS_2 networks.[24] In simple models describing trap-limited photoconductivity, the exponent, γ, is a measure of the depth of the traps below (above) the conduction (valence) band for an n-type (p-type) system.[24] We see no consistent trend of γ with nanosheet content, which implies the presence of graphene has no significant effect on the trap profile. One interesting point (which we discuss below) is that while the absolute increase in conductivity is considerably larger for the 16wt% sample (~4 mS/m vs. ~40 μS/m, at 200 mW/cm^2), the fractional increase in conductivity is much smaller for the composite sample (~1% vs. ~70%, at 200 mW/cm^2).

In conductor-insulator composites, the (dark) conductivity as a function of conductive filler volume fraction (ϕ) is usually described by percolation theory.[25] An important parameter in this theory is the percolation threshold, ϕ_c, which is the filler volume-fraction where the first continuous conductive path appears. Above the percolation threshold, the (dark) conductivity increases rapidly with filler content: $\sigma_D \propto (\phi - \phi_c)^n$, where n is usually >2.[25-27] Above the percolation threshold, quite high conductivities can result as the current flows solely through

the conducting network and is limited only by interparticle charge transfer. It is this regime which is the topic of the vast majority of papers on electrical percolation in composites. Conversely, the regime below the percolation threshold, where $\phi<\phi_c$, is much less studied. In this range, the filler particles are either isolated or aggregated in small clusters with no continuous paths of conductive filler. As a result, we can imagine two contributions to current flow; one solely through the insulating matrix and one which alternates through insulating and conducting sections which are arranged in series. If the matrix conductivity is very low, we would expect the former case to contribute very little to the conductivity. In the latter case, one can view charge carriers as travelling slowly in the insulating regions and rapidly in the conducting portions resulting in a decrease in carrier transit time as the filler content is increased.[21] As a result, the latter contribution becomes more and more dominant as the conductive volume fraction increases, leading to a ϕ-dependent conductivity which is usually modelled using:[26, 28, 29]

$$\sigma_D = \sigma_M \left[\frac{\phi_c - \phi}{\phi_c} \right]^{-s} \tag{1}$$

where σ_M is the (dark) conductivity of the insulating matrix, s is the percolation exponent and $(\phi_c - \phi)/\phi_c$ is referred to as the reduced percolation threshold.

In such composites, we would expect current flow to be spatially inhomogeneous and be dominated by paths of least resistance. Such low resistance pathways are those which minimise the portion of the journey through the matrix and maximise the number of traversed graphene nanosheets, resulting in low transit times. One would expect the network of paths of least resistance which contribute significantly to current flow to be very sensitive to the graphene loading level. This might lead to a highly nonlinear ϕ-dependence (i.e s>1) with the actual value of s reflecting the structure of the emergent conducting network.

It is worth noting that, in this work, we are dealing with networks which contain both MoS_2 and graphene nanosheets. In any network, the conductivity is partially limited by the effective resistance associated with carriers hopping/tunnelling from nanosheet to nanosheet.[20] It is not yet clear what the magnitude of the junction resistance is or how it differs between MoS_2-graphene, MoS_2-MoS_2 or graphene-graphene junctions. In fact, very little is known about inter-nanosheet charge transport. However, for single component networks of MoS_2, the conductivity has been measured at ~10^{-6}-10^{-5} S/m while graphene-only networks display ~10^4

S/m, a difference of ~9-10 orders of magnitude.[22, 23] This implies that, as long as the probability of MoS$_2$-graphene charge transfer is not prohibitively low, the addition of graphene will result in significant conductivity increases.

For the printed composites described here, the dark conductivity versus graphene mass fraction data (reproduced in Figure 3A) shows a smooth increase to a maximum value of ~1 S/m at 16 wt% graphene. As the observed conductivities are relatively low and because no sharp conductivity increase was observed, we can conclude that all samples are below the percolation threshold. This implies the percolation threshold is much higher than the values of ~1% usually observed in graphene-polymer composites.[30] However, this data is consistent with previous work on MoS$_2$/graphene composites and in line with theory which suggests that percolation thresholds can be high in systems of aligned discs.[22] If our samples are all in the pre-percolation regime (i.e. $\phi<\phi_c$), no continuous graphene-only conductive paths are available. This is important as it means that here, all current flow will involve some transit via sections of MoS$_2$.

If these composite channels are indeed below the percolation threshold, then Equation 1 should apply. However, to properly analyse these composites, the mass fraction, M_f, must be converted to volume fraction, ϕ. Although this conversion is trivial in polymer-matrix composites, only requiring knowledge of matrix and filler densities, it is less straightforward in nano:nano composites such as these because of the presence of porosity.[20] In relatively thick nano:nano composite films, the volume fraction can be found if the film density is known ($\phi = M_f \rho_{film} / \rho_{filler}$) but for thin printed channels such as these, measurement of the density is not trivial. To address this, we have derived a simple equation for the filler volume fraction in two-phase composites which include porosity (defined by a fractional porous volume, P, see SI):

$$\phi = \frac{(1-P)}{1+(1/M_f -1)\rho_G / \rho_M} \tag{2a}$$

where ρ_M=5060 kg/m^3 and ρ_G=2200 kg/m^3 are the densities of the matrix (MoS$_2$) and filler (graphene) respectively. We note that we define the volume fraction as the volume of graphene divided by the total film volume including pore volume (see SI).

However, because we do not know the porosity, P, this equation cannot be used directly to transform M_f into ϕ. To resolve this, we use Equation 2a to relate the reduced percolation threshold to the graphene mass fraction in porous composites (see SI):

$$\frac{\phi_c - \phi}{\phi_c} = \frac{1 - M_f / M_{f,c}}{1 + M_f (\rho_M / \rho_G - 1)} \qquad (2b)$$

where $M_{f,c}$ is the mass fraction equivalent of the percolation threshold. This equation relies on the assumption that the porosity does not change with volume fraction, which should hold true when both filler and matrix have similar geometries.

To test the validity of Equation 1, we calculated the reduced volume fraction for different values of $M_{f,c}$. In each case, we plotted the measured dark conductivity versus $(\phi_c - \phi)/\phi_c$ to find the value of $M_{f,c}$ which gave the most reasonable fit. In this way, we found a well-defined power relationship between σ_D and $(\phi_c - \phi)/\phi_c$ when we take $M_{f,c}$=0.25 (Figure 3B). Fitting Equation 1 (solid line) then gave a percolation exponent of s=7.6, in reasonable agreement with a previously reported value of s=5.2.[22] While it is impossible to convert $M_{f,c}$ into volume fraction (i.e. ϕ_c) without knowing the film porosity, we note that nanosheet networks generally have porosity close to 50%,[20] allowing us to estimate ϕ_c ~22vol%, very close to the value of ~23vol%, previously reported for MoS$_2$-graphene composites.[22] In addition, we can use Equation 2b to express Equation 1 in terms of M_f, allowing us to plot the percolation fit in Figure 3A, yielding very good agreement as shown by the solid line.

While electrical percolation in MoS$_2$-graphene composites has been observed previously, photoconductivity in such systems has not. Figure 3C shows the photoconductivity (i.e. the conductivity increase on illumination), measured at 206 mW/cm^2 using a λ=511 nm laser, plotted versus the mass fraction of graphene in the channel. We find a two order increase in photoconductivity from ~4×10^{-5} S/m for the MoS$_2$-only channel to ~4×10^{-3} S/m for the 16 wt% graphene channel. It is clear that adding graphene below the percolation threshold results in large increases in photoconductivity. This is probably because photo-induced charge carriers can travel rapidly to the electrodes due to the higher channel mobility conferred by the addition of graphene. This indicates that the photoconductivity could be tuned over a relatively wide range, simply by control of the graphene content in composites such as these.

However, by comparison of Figures 3A and 3C, it is clear that the photoconductivity increases significantly more slowly than the dark conductivity as the graphene content is

increased. To explain this, we consider both dark and illuminated composite conductivity in terms of carrier density and mobility; $\sigma_D = q n_D \mu_D$ and $\sigma = q n \mu$, where q is the carrier charge, n_D and n are the dark and illuminated effective carrier densities and μ_D and μ are the dark and illuminated mobilities. Under illumination, photocarriers are generated in the MoS$_2$ and the carrier density becomes $n = n_D + \Delta n$ at steady state where Δn is the photoinduced carrier density. Then, assuming the mobility is not changed significantly under illumination (i.e. $\mu_D \approx \mu$), the photoconductivity can be written as $\sigma - \sigma_D = q \mu_D \Delta n$.

In the dark, we expect both mobility (μ_D) and carrier density (n_D) to increase with graphene content,[31] with the mobility increase due to the effect of graphene on transit time described above.[21] however, we must also consider that the graphene sheets will generally have a much higher free carrier density than the MoS$_2$, leading to an increase in the effective carrier density as graphene content increases. In a percolating system, we might expect both carrier density and mobility follow percolation-like scaling laws. While this has not been reported to our knowledge, reanalysing the data of Tan et al.[31] shows this to be approximately true. Assuming this is the case, we can write:

$$n_D = n_M \left[\frac{\phi_c - \phi}{\phi_c} \right]^{-N} , \quad \mu_D = \mu_M \left[\frac{\phi_c - \phi}{\phi_c} \right]^{-M} \tag{3a}$$

where n_M and μ_M are the dark carrier density and mobility of the matrix (MoS$_2$). This means that the dark conductivity can be written as

$$\sigma_D = q n_M \mu_M \left[\frac{\phi_c - \phi}{\phi_c} \right]^{-(N+M)} \tag{3b}$$

This shows that the ϕ-dependence of the dark conductivity has contributions from both mobility and carrier density and, by comparison with Equation 1, means that s=N+M.

Turning to the photoconductivity, we would expect the photo-induced carrier density, Δn, to depend weakly on graphene content below percolation since the main effect of the graphene is to reduce the amount of MoS$_2$ available to generate photocarriers, i.e. $\Delta n \propto 1 - \phi$. Approximating Δn as independent of ϕ allows us to write the photoconductivity as:

$$\sigma - \sigma_D \approx q \Delta n \mu_M \left[\frac{\phi_c - \phi}{\phi_c} \right]^{-M} \tag{4a}$$

This expression implies that, at this level of approximation, the ϕ-dependence of the photoconductivity has a contribution from the mobility but not the carrier density. In addition, it implies percolation-like scaling behaviour. To test this, in Figure 3D we plot photoconductivity versus reduced volume fraction, calculated using the same percolation threshold as was found for the dark conductivity ($M_{f,c}$=25wt%, ϕ_c~22vol%). As predicted by Equation 4a, we find good linearity, consistent with M=3.8, implying that the data in Figure 3C reflect the dependence of mobility on graphene content.

The data in Figure 3C show the photoconductivity increasing by 100× between the MoS_2-only and 16wt% channels. Such an increase is consistent with previous work which showed that the mobility of organic devices could be increased by up to 1000× by adding graphene.[21] The mobility of an MoS_2 nanosheet network has been quoted as ~0.1 cm^2/Vs,[20] implying the network mobility of the 16wt% composite to be as high as ~10 cm^2/Vs. If this inferred value were correct, the mobility of these simple devices would be competitive with the best printed organic devices.[3]

The fact that the photoconductivity increases less rapidly with graphene content than the dark conductivity means the fractional photoconductivity, $(\sigma - \sigma_D)/\sigma_D$, decays with mass fraction. This data is plotted in Figure 3E and shows a rapid fall-off in $(\sigma - \sigma_D)/\sigma_D$ with M_f, falling from ~0.7 for the MoS_2-only channel to ~0.01 for the 16wt% sample. Combining Equations 3b and 4a predicts the fractional photoconductivity to scale with reduced volume fraction as

$$\frac{\sigma - \sigma_D}{\sigma_D} = \frac{\Delta n}{n_M} \left[\frac{\phi_c - \phi}{\phi_c} \right]^N \tag{4b}$$

Figure 3F plots the fractional photoconductivity versus reduced volume fraction, calculated using the same percolation threshold found for the dark conductivity ($M_{f,c}$=25wt%, ϕ_c~22vol%). As predicted by Equation 4b, percolation-like scaling is observed, consistent with N=3.7. Again, this means the data in Figure 3E reflects the increase in dark carrier density with increasing graphene content. Because the carrier density of an MoS_2 network has been reported at ~10^{12} cm^{-3},[20] the 100-fold reduction in fractional photoconductivity implies the 16wt% sample has a carrier density of ~10^{14} cm^{-3}.

In addition, Equation 4b implies that the fractional photoconductivity will approach zero as the percolation threshold is approached. This is as expected given that the amount of

current flowing through the MoS_2 should be negligible compared to the current flowing through the graphene above the percolation threshold.

These data suggest that the increase in dark conductivity with graphene content below the percolation threshold is due to graphene-induced increases in both mobility and effective carrier density. The similarity of the N and M exponents indicates that the relative contributions of mobility and carrier density are comparable in magnitude. However, the graphene content dependence of the photoconductivity depends only on the graphene-induced mobility increase. Similarly, the M_f dependence of the fractional photoconductivity depends only on the graphene-induced carrier density increase. As a result, measuring the photoconductivity in such composites is a useful way to differentiate the effects of filler content on mobility and carrier density, parameters which are usually aggregated in the conductivity.

In conclusion, this work shows that all-printed, all-nanosheet devices can be fabricated where the active channel is a composite material and the graphene electrodes contribute negligible series resistance. Both dark- and photo-conductivity are described by percolation theory with the photoconductivity reflecting the increase in channel mobility associated with the graphene. It is possible that these results could be translated to other device types. One possibility might be to fabricate transistor channels from MoS_2/graphene composite networks where the addition of graphene would be expected to increase the mobility, albeit at the likely cost of increased off currents.
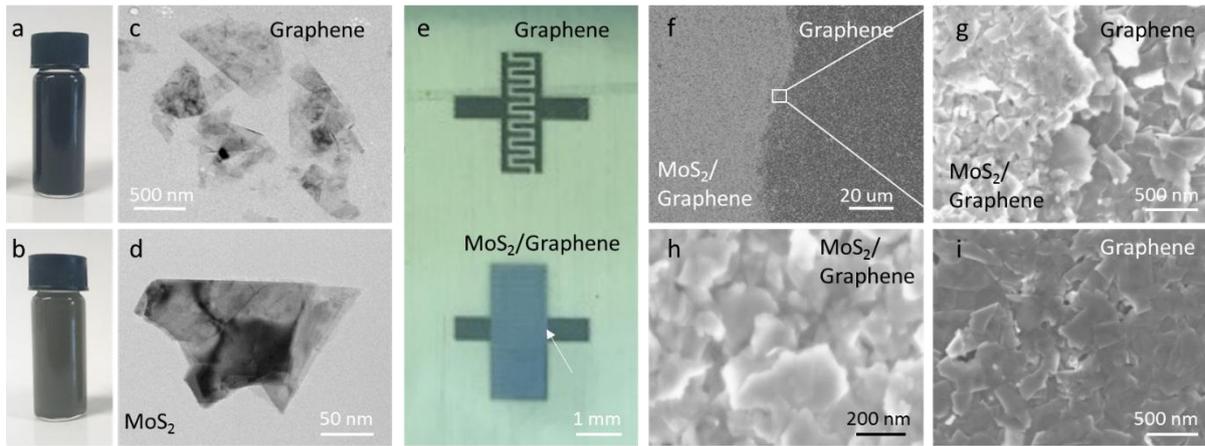
Figure 1: a-b) Photographs of nanosheet dispersions in NMP of (a) graphene and (b) MoS_2. c-d) Representative TEM images of exfoliated nanosheets of (c) graphene and (d) MoS_2. e) Micrograph showing interdigitated graphene electrodes before (top) and after (bottom) printing of the MoS_2/graphene composite (M_f=5%) channel. The arrow indicates the position where the SEM images in (f) and (g) were collected. f-g) Low-resolution (f) and high resolution (g) SEM images of composite/graphene interface (collected from position marked by arrow in e). h-i) Representative SEM images of portions of the device printed from MoS_2/graphene composite (M_f=5%, h) and graphene (i) nanosheets.
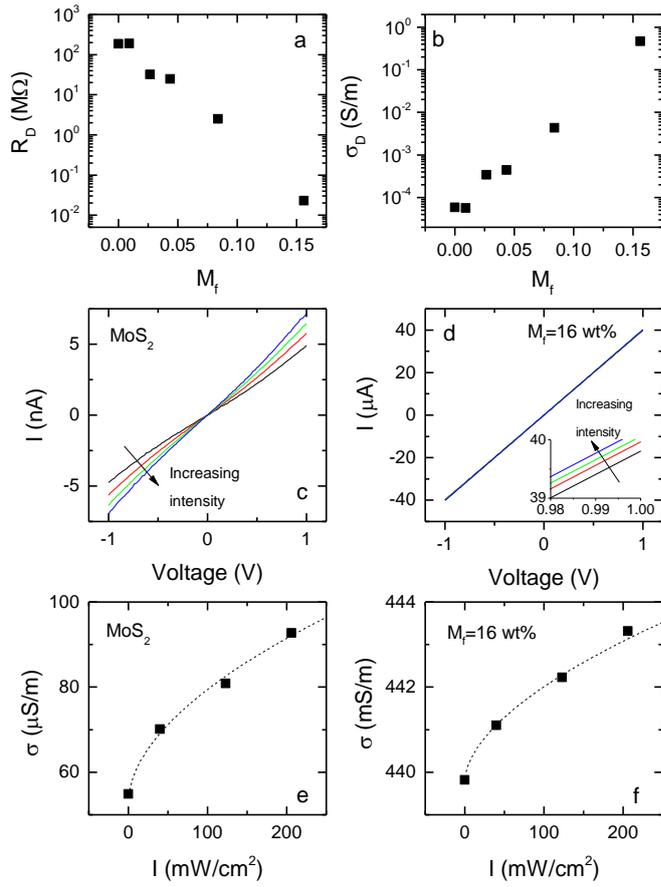
Figure 2: a-b) Device resistance (a) and channel conductivity (b) as a function of the mass fraction of graphene nanosheets in the composite channel, both measured in the dark. c-d) Current-voltage characteristics for devices with (c) an MoS_2-only channel and (d) an MoS_2/graphene composite (M_f=16%) channel. The inset in (d) shows a small but well defined intensity dependence. e-f) Light intensity-dependent conductivity for devices with (e) an MoS_2-only channel and (f) an MoS_2/graphene composite (M_f=16%) channel.
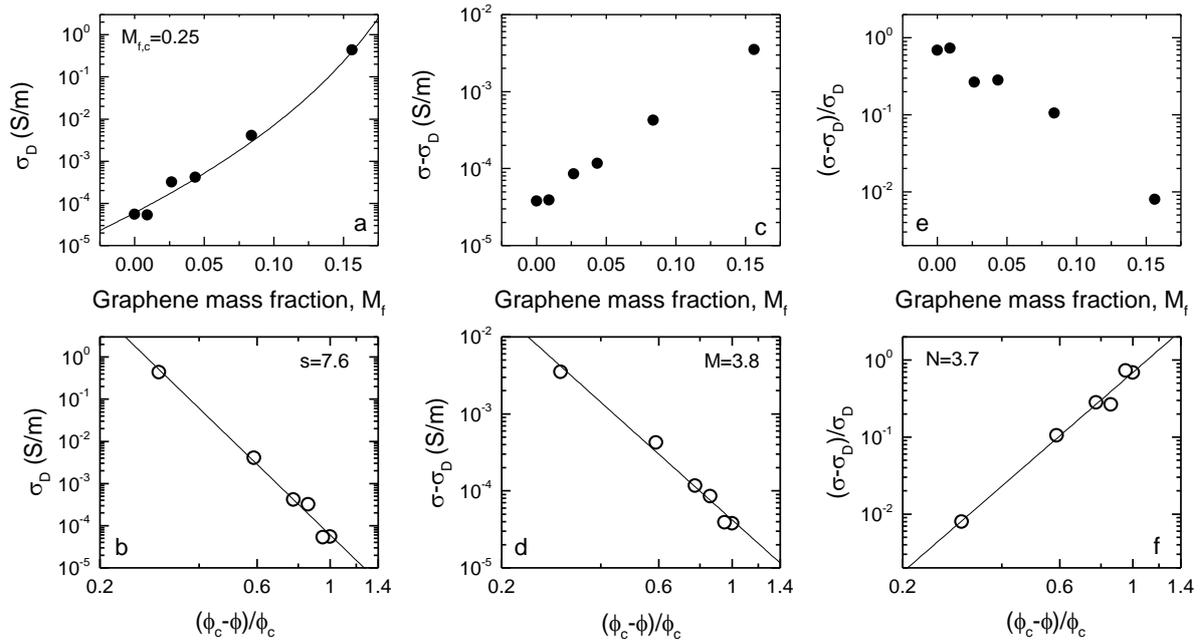
Figure 3: Dark conductivity, σ_D, (a, b), photoconductivity (c, d) and fractional photoconductivity (e, f) plotted versus graphene mass fraction (top row) and reduced volume fraction (bottom row). In c-f, the conductivity under illumination, σ, was measured at an incident intensity of 206 mW/cm^2 using a 511 nm laser. In the bottom row, the reduced volume fraction is defined as $(\phi_c - \phi)/\phi_c$ where ϕ and ϕ_c are the graphene volume fraction and the percolation threshold respectively. The solid lines represent the predictions of percolation theory. The mass fraction equivalent of the percolation threshold was $M_{f,c}$=25wt%.

References

1.   Burroughes, J. H.; Bradley, D. D. C.; Brown, A. R.; Marks, R. N.; Mackay, K.; Friend, R. H.; Burn, P. L.; Holmes, A. B., Light-Emitting-Diodes Based on Conjugated Polymers. *Nature* **1990,** 347, 539-541.
2.   Jarrett, C. P.; Friend, R. H.; Brown, A. R.; Deleeuw, D. M., Field-Effect Measurements in Doped Conjugated Polymer-Films - Assessment of Charge-Carrier Mobilities. *Journal of Applied Physics* **1995,** 77, 6289-6294.
3.   Baeg, K. J.; Caironi, M.; Noh, Y. Y., Toward Printed Integrated Circuits Based on Unipolar or Ambipolar Polymer Semiconductors. *Advanced Materials* **2013,** 25, 4210-4244.
4.   Yang, J.; Choi, M. K.; Kim, D.-H.; Hyeon, T., Designed Assembly and Integration of Colloidal Nanocrystals for Device Applications. *Advanced Materials* **2016,** 28, 1176-1207.
5.   Zaumseil, J., Single-Walled Carbon Nanotube Networks for Flexible and Printed Electronics. *Semiconductor Science and Technology* **2015,** 30, 074001.
6.   Deng, Y. X.; Luo, Z.; Conrad, N. J.; Liu, H.; Gong, Y. J.; Najmaei, S.; Ajayan, P. M.; Lou, J.; Xu, X. F.; Ye, P. D., Black Phosphorus-Monolayer Mos2 Van Der Waals Heterojunction P-N Diode. *ACS Nano* **2014,** 8, 8292-8299.
7.   Bandurin, D. A.; Tyurnina, A. V.; Yu, G. L.; Mishchenko, A.; Zolyomi, V.; Morozov, S. V.; Kumar, R. K.; Gorbachev, R. V.; Kudrynskyi, Z. R.; Pezzini, S.; Kovalyuk, Z. D.; Zeitler, U.; Novoselov, K. S.; Patane, A.; Eaves, L.; Grigorieva, I. V.; Fal'ko, V. I.; Geim, A. K.; Cao, Y., High

Electron Mobility, Quantum Hall Effect and Anomalous Optical Response in Atomically Thin Inse. *Nat. Nanotechnol.* **2017,** 12, 223-+.

8.   Coleman, J. N.; Lotya, M.; O'Neill, A.; Bergin, S. D.; King, P. J.; Khan, U.; Young, K.; Gaucher, A.; De, S.; Smith, R. J.; Shvets, I. V.; Arora, S. K.; Stanton, G.; Kim, H. Y.; Lee, K.; Kim, G. T.; Duesberg, G. S.; Hallam, T.; Boland, J. J.; Wang, J. J.*, et al.*, Two-Dimensional Nanosheets Produced by Liquid Exfoliation of Layered Materials. *Science* **2011,** 331, 568-571.

9.   Paton, K. R.; Varrla, E.; Backes, C.; Smith, R. J.; Khan, U.; O'Neill, A.; Boland, C.; Lotya, M.; Istrate, O. M.; King, P.; Higgins, T.; Barwich, S.; May, P.; Puczkarski, P.; Ahmed, I.; Moebius, M.; Pettersson, H.; Long, E.; Coelho, J.; O'Brien, S. E.*, et al.*, Scalable Production of Large Quantities of Defect-Free Few-Layer Graphene by Shear Exfoliation in Liquids. *Nature Materials* **2014,** 13, 624-630.

10.   Backes, C.; Szydlowska, B. M.; Harvey, A.; Yuan, S.; Vega-Mayoral, V.; Davies, B. R.; Zhao, P. L.; Hanlon, D.; Santos, E. J.; Katsnelson, M. I.; Blau, W. J.; Gadermaier, C.; Coleman, J. N., Production of Highly Monolayer Enriched Dispersions of Liquid-Exfoliated Nanosheets by Liquid Cascade Centrifugation. *ACS Nano* **2016,** 10, 1589-601.

11.   Harvey, A.; Backes, C.; Gholamvand, Z.; Hanlon, D.; McAteer, D.; Nerl, H. C.; McGuire, E.; Seral-Ascaso, A.; Ramasse, Q. M.; McEvoy, N.; Winters, S.; Berner, N. C.; McCloskey, D.; Donegan, J. F.; Duesberg, G. S.; Nicolosi, V.; Coleman, J. N., Preparation of Gallium Sulfide Nanosheets by Liquid Exfoliation and Their Application as Hydrogen Evolution Catalysts. *Chemistry of Materials* **2015,** 27, 3483-3493.

12.   Harvey, A.; He, X. Y.; Godwin, I. J.; Backes, C.; McAteer, D.; Berner, N. C.; McEvoy, N.; Ferguson, A.; Shmeliov, A.; Lyons, M. E. G.; Nicolosi, V.; Duesberg, G. S.; Donegan, J. F.; Coleman, J. N., Production of Ni(Oh)(2) Nanosheets by Liquid Phase Exfoliation: From Optical Properties to Electrochemical Applications. *Journal of Materials Chemistry A* **2016,** 4, 11046-11059.

13.   McManus, D.; Vranic, S.; Withers, F.; Sanchez-Romaguera, V.; Macucci, M.; Yang, H.; Sorrentino, R.; Parvez, K.; Son, S.-K.; Iannaccone, G.; Kostarelos, K.; Fiori, G.; Casiraghi, C., Water-Based and Biocompatible 2d Crystal Inks for All-Inkjet-Printed Heterostructures. *Nature Nanotechnology* **2017,** advance online publication.

14.   Torrisi, F.; Hasan, T.; Wu, W.; Sun, Z.; Lombardo, A.; Kulmala, T. S.; Hsieh, G.-W.; Jung, S.; Bonaccorso, F.; Paul, P. J.; Chu, D.; Ferrari, A. C., Inkjet-Printed Graphene Electronics. *ACS Nano* **2012,** 6, 2992-3006.

15.   Chen, G. H.; Yu, Y. Q.; Zheng, K.; Ding, T.; Wang, W. L.; Jiang, Y.; Yang, Q., Fabrication of Ultrathin Bi2s3 Nanosheets for High-Performance, Flexible, Visible-Nir Photodetectors. *Small* **2015,** 11, 2848-2855.

16.   Ghosh, S.; Winchester, A.; Muchharla, B.; Wasala, M.; Feng, S. M.; Elias, A. L.; Krishna, M. B. M.; Harada, T.; Chin, C.; Dani, K.; Kar, S.; Terrones, M.; Talapatra, S., Ultrafast Intrinsic Photoresponse and Direct Evidence of Sub-Gap States in Liquid Phase Exfoliated Mos2 Thin Films. *Scientific Reports* **2015,** 5.

17.   Mahjouri-Samani, M.; Gresback, R.; Tian, M. K.; Wang, K.; Puretzky, A. A.; Rouleau, C. M.; Eres, G.; Ivanov, I. N.; Xiao, K.; McGuire, M. A.; Duscher, G.; Geohegan, D. B., Pulsed Laser Deposition of Photoresponsive Two-Dimensional Gase Nanosheet Networks. *Advanced Functional Materials* **2014,** 24, 6365-6371.

18.   Withers, F.; Yang, H.; Britnell, L.; Rooney, A. P.; Lewis, E.; Felten, A.; Woods, C. R.; Romaguera, V. S.; Georgiou, T.; Eckmann, A.; Kim, Y. J.; Yeates, S. G.; Haigh, S. J.; Geim, A. K.; Novoselov, K. S.; Casiraghi, C., Heterostructures Produced from Nanosheet-Based Inks. *Nano Letters* **2014,** 14, 3987-3992.

19.   Finn, D. J.; Lotya, M.; Cunningham, G.; Smith, R. J.; McCloskey, D.; Donegan, J. F.; Coleman, J. N., Inkjet Deposition of Liquid-Exfoliated Graphene and Mos2 Nanosheets for Printed Device Applications. *Journal of Materials Chemistry C* **2014,** 2, 925-932.

20.   Kelly, A. G.; Hallam, T.; Backes, C.; Harvey, A.; Esmaeily, A. S.; Godwin, I.; Coelho, J.; Nicolosi, V.; Lauth, J.; Kulkarni, A.; Kinge, S.; Siebbeles, L. D. A.; Duesberg, G. S.; Coleman, J. N., All-Printed Thin-Film Transistors from Networks of Liquid-Exfoliated Nanosheets. *Science* **2017,** 356, 69-72.

21.   Pathipati, S. R.; Pavlica, E.; Schlierf, A.; El Gemayel, M.; Samori, P.; Palermo, V.; Bratina, G., Graphene-Induced Enhancement of N-Type Mobility in Perylenediimide Thin Films. *J. Phys. Chem. C* **2014,** 118, 24819-24826.

22.   Cunningham, G.; Lotya, M.; McEvoy, N.; Duesberg, G. S.; van der Schoot, P.; Coleman, J. N., Percolation Scaling in Composites of Exfoliated Mos2 Filled with Nanotubes and Graphene. *Nanoscale* **2012,** 4, 6260-6264.

23.   De, S.; Coleman, J. N., Are There Fundamental Limitations on the Sheet Resistance and Transmittance of Thin Graphene Films? *Acs Nano* **2010,** 4, 2713-2720.

24.   Cunningham, G.; Hanlon, D.; McEvoy, N.; Duesberg, G. S.; Coleman, J. N., Large Variations in Both Dark- and Photoconductivity in Nanosheet Networks as Nanomaterial Is Varied from Mos2 to Wte2. *Nanoscale* **2015,** 7, 198-208.

25.   Bauhofer, W.; Kovacs, J. Z., A Review and Analysis of Electrical Percolation in Carbon Nanotube Polymer Composites. *Composites Science and Technology* **2009,** 69, 1486-1498.

26.   Stauffer, D.; Aharony, A., *Introduction to Percolation Theory*. 2nd ed.; Taylor & Francis: London, 1985.

27.   Wu, J. J.; McLachlan, D. S., Percolation Exponents and Thresholds Obtained from the Nearly Ideal Continuum Percolation System Graphite-Boron Nitride. *Physical Review B* **1997,** 56, 1236-1248.

28.   Chiteme, C.; McLachlan, D. S.; Sauti, G., Ac and Dc Percolative Conductivity of Magnetite-Cellulose Acetate Composites. *Physical Review B* **2007,** 75, 094202.

29.   Clerc, J. P.; Giraud, G.; Laugier, J. M.; Luck, J. M., The Ac Electrical-Conductivity of Binary Disordered-Systems, Percolation Clusters, Fractals and Related Models. *Advances in Physics* **1990,** 39, 191-308.

30.   Stankovich, S.; Dikin, D. A.; Dommett, G. H. B.; Kohlhaas, K. M.; Zimney, E. J.; Stach, E. A.; Piner, R. D.; Nguyen, S. T.; Ruoff, R. S., Graphene-Based Composite Materials. *Nature* **2006,** 442, 282-286.

31.   Tan, H.-x.; Xu, X.-c., Conductive Properties and Mechanisms of Different Polymers Doped by Carbon Nanotube/Polypyrrole 1d Hybrid Nanotubes. *RSC Advances* **2015,** 5, 61383-61389.

Supporting information

Tuneable photoconductivity and mobility enhancement in printed MoS$_2$/graphene composites

Adam Kelly, Conor Murphy, Andrew Harvey, Amir Sajad Esmaeily, David McCloskey, Jonathan N. Coleman[*]

School of Physics, CRANN and AMBER Research Centers, Trinity College Dublin, Dublin 2, Ireland.

*colemaj@tcd,ie

Calculation of volume fraction and reduced volume fraction

The mass fraction is related to the volume fraction by:

$$M_f = \frac{M_G}{M_T} = \frac{\rho_G V_G}{\rho_T V_T} = \frac{\rho_G}{\rho_T}\phi$$

where the symbols M, V and ρ refer to mass, volume and density and the subscripts G, T and M refer to graphene, total and MoS2. Thus M_G is the mass of graphene in the sample. We note that here we define the volume fraction as the volume of all graphene divided by the entire film volume (including porous volume).

In a porous film, the film density is given by

$$\rho_T = \frac{M_T}{V_T} = \frac{M_G + M_M}{V_G + V_M + V_{pore}} = \frac{M_G + M_M}{M_G / \rho_G + M_M / \rho_M + PV_T} = \frac{M_G + M_M}{M_G / \rho_G + M_M / \rho_M + PM_T / \rho_T}$$

where P is the porosity (fractional pore volume, i.e. $P = V_{pores} / V_{film}$)

Rearranging:

$$\rho_T = \frac{(1-P)}{M_f / \rho_G + (1-M_f) / \rho_M}$$

Then

$$\phi = \frac{\rho_T}{\rho_G} M_f$$

and

$$\phi = \frac{(1-P)}{1+(1/M_f - 1)\rho_G / \rho_M}$$

The reduced volume fraction is given by $\dfrac{\phi_c - \phi}{\phi_c}$

This can be written as

$$\frac{\phi_c - \phi}{\phi_c} = 1 - \frac{\left[\dfrac{(1-P)}{1+(1/M_f - 1)\rho_G / \rho_M}\right]}{\left[\dfrac{(1-P)}{1+(1/M_{f,c} - 1)\rho_G / \rho_M}\right]}$$

Where $M_{f,c}$ is the mass fraction associated with the percolation threshold. Rearranging:

$$\frac{\phi_c - \phi}{\phi_c} = \frac{1 - M_f / M_{f,c}}{1 + M_f (\rho_M / \rho_G - 1)}$$